Program at a Glance

※ **Click the session title to see detailed schedules.**
※ **[SS] : Special Session**

Final Program

as of November 25, 2025

	Time	Room C (Samda A)	Room D (Samda B)	Room E (301)	Room F (302)	3F Lobby
Dec. 2 (Tue.)	09:00-12:00	**[WS1-1] Workshop** "Metrology for 6G: Accurate Measurements at mm-Wave and Sub-THz Frequencies"	**[WS2-1] Workshop** "Recent Advance of THz Integrated Circuits"	**[WS3] Workshop** "III-V Device Modeling Trends and Large Signal Characterization"	**[WS5] Workshop** "Filters and Metamaterial Circuits for Satellites and Wireless Systems"	
	12:00-13:00	Lunch (3F, Delizia)				
	13:00-15:30	**[WS1-2] Workshop** "Metrology for 6G: Accurate Measurements at mm-Wave and Sub-THz Frequencies"	**[WS2-2] Workshop** "Recent Advance of THz Integrated Circuits"	**[WS4-1] Workshop** "Advancing 5G/6G ORAN, MIMO and RIS Research and Development"	**[WS6-1] Workshop** "High-Gain and Wideband Microwave Superconducting Parametric Amplifiers for High-Fidelity Quantum Bit Readout"	
	15:30-15:45	Coffee Break				
	15:45-18:15	**[WS1-3] Workshop** "Metrology for 6G: Accurate Measurements at mm-Wave and Sub-THz Frequencies"		**[WS4-2] Workshop** "Advancing 5G/6G ORAN, MIMO and RIS Research and Development"	**[WS6-2] Workshop** "High-Gain and Wideband Microwave Superconducting Parametric Amplifiers for High-Fidelity Quantum Bit Readout"	
	18:15-18:30	Break				
	18:30-19:30	**Welcome Reception** (5F, Ocean View)				

	Time	Room A (Halla A)	Room B (Halla B)	Room C (Samda A)	Room D (Samda B)	Room E (301)	Room F (302)	Room G (303)	3F Lobby
Dec. 3 (Wed.)	08:30-08:50	**Opening Ceremony** (3F, Halla A+B)							**Exhibition** (08:30-17:30)
	08:50-09:35	**Keynote Speech I** (3F, Halla A+B) "Space Exploration and Our Place in the Universe" **Dr. Goutam Chattopadhyay** (JPL, USA)							
	09:35-10:20	**Keynote Speech II** (3F, Halla A+B) "Advances in Millimeter-Wave Circuit Design for Future Communications" **Prof. Kenichi Okada** (Institute of Science Tokyo, Japan)							
	10:20-10:30	Break							
	10:30-11:15	**Keynote Speech III** (3F, Halla A+B) "Mode-Oriented Element-Level Beamforming: A New Paradigm for Radiation Manipulation" **Prof. Quan Xue** (South China Univ. of Technology, China)							
	11:15-12:00	**Keynote Speech IV** (3F, Halla A+B) "Next Generation Communications Technology:The Foundation for New Convergence Services" **Dr. Yongsoon Baek** (ETRI, Korea)							
	12:00-13:20	Lunch (5F, Tamna B+C)							
	13:20-15:00	**WA1** RF Circuit Techniques for Wideband and Multi-Band Systems	**WB1** [SS] Innovative Front-End Components in mmWave IC Design	**WC1** "Ask us Anything" Session	**WD1** Millimeter-Wave and Compact Antenna Technologies	**WE1** EMC Security and Modeling	**WF1** mmWave Phased Array Antenna System	**WG1** Radar Hardware and Systems	
	15:00-15:40	Coffee Break							**Interactive Forum I (Poster)** 15:00-16:40
	15:40-17:20	**WA2** [SS] Joint APMC/EuMC Special Session	**WB2** Advances in Millimeter Wave and THz Phased Array Ics	**WC2** Young Professionals (YP)	**WD2** Antenna Measurement, Imaging, and Performance Engineering	**WE2** [SS] EMC Test and Noise Reduction	**WF2** Sub-THz Communication for 6G	**WG2** Radar Signal Processing, Measurement Techniques and Systems	
	17:20-17:30	Break							
	17:30-18:20		**IEEE MTT-s BPC Panel Session** (17:30-18:30)	**YP/WiM Social Network (5F, Ocean View)**					

Dec. 4 (Thu.)	Time	Room A (Halla A)	Room B (Halla B)	Room C (Samda A)	Room D (Samda B)	Room E (301)	Room F (302)	Room G (303)	3F Lobby
	08:30-10:10	**TA1**	**TB1**	**TC1**	**TD1**	**TE1**	**TF1**	**TG1**	**Exhibition** (08:30-18:00) &

		Millimeter-Wave and 5G RFIC Innovations	High Performance Power Amplifiers	Next-Generation RF and Antenna Technologies for Strategic Defense and Emergency Response	Space-Time Coding & Reconfigurable Antennas for Future Wireless Systems	Next-Generation Antenna Architectures: Lenses, Arrays, and Machine Learning	Reconfigurable Intelligent Surface for 5G adv/6G	Algorithms and Computational EM for Intelligent EW/Sensing		**Student Design Competition**
10:10-10:30		Coffee Break								
10:30-12:10	**TA2**	**TB2**	**TC2**	**TD2**	**TE2**	**TF2**	**TG2**			
	RF Front-End Circuits for Reconfigurable and mmWave Applications	Millimeter-Wave Power Amplifiers	Meet the Editors	SIW, Multibeam, and Biomedical Antenna Solutions	[SS] AI and Emerging Techniques in Antenna Design for IoT and Microwave Systems	Advanced Front-End System for 5G adv/6G	[SS] Emerging Electromagnetic Technologies for Medical Diagnosis and Therapy			
12:10-13:20	Lunch (5F, Tamna B+C)									
13:20-15:00	**TA3**	**TB3**	**TC3**	**TD3**	**TE3**	**TF3**	**TG3**			
	RF Power Amplifier	Millimeter Wave and Sub-Teraherz Signal Sources	Industry Session	Filtering and ME Dipole Antenna Technologies	Recent Advances in Microwave Components and Their Applications	RF and Antenna Technologies for Satellite Communications	RF and Microwave for Medical Applications			
15:00-15:40	Coffee Break							**Interactive Forum II (Poster)** 15:00-16:40		
15:40-17:20	**TA4**	**TB4**	**TC4**	**TD4**	**TE4**	**TF4**	**TG4**			
	Millimeter Wave Front-End Amplifiers	Signal Generation & Frequency Conversion	Women in Microwaves (WiM)	Wide-Scanning and Reconfigurable Antenna Systems	Design and Characterization of RF Systems and Components	Radar Applications in Human and Environmental Sensing	Innovations in Antenna Design and Electromagnetic Tracking			
17:20-18:00	Break									
18:00-20:00	**Banquet** (Woojung Hall, Booyoung Hotel & Resort)									

Dec. 5 (Fri.)	Time	Room A (Halla A)	Room B (Halla B)	Room C (Samda A)	Room D (Samda B)	Room E (301)	Room F (302)	Room G (303)	3F Lobby	
		FA1	**FB1**		**FD1**	**FE1**	**FF1**	**FG1**		**Exhibition** (08:30-13:20)
	08:30-10:10	Advances in Millimeter Wave Transceivers	Simulation and Measurement Techniques		Reconfigurable Antennas, Metasurfaces, and Intelligent Array Systems	Antenna Designs: Reconfigurability, Feed Networks, and RCS Reduction	Advances in Wireless Sensors and Applications	[SS] Recent Advances in Radar Research for Various Applications I		
	10:10-10:30	Coffee Break								
	10:30-12:10	**FA2**	**FB2**	**FC2**	**FD2**	**FE2**	**FF2**	**FG2**		
		[SS] Advanced Components for 5G/6G	Recent Advances in Instrumentation and Device Measurements	Innovations and Challenges in Terahertz Engineering	AI and Physics-Based Approaches for RF/Microwave Component Design	Cutting-Edge Array Design: Performance Optimization and Measurement	[SS] AI-Driven Design and Signal Processing in RF, mmWave, and THz Systems	[SS] Recent Advances in Radar Research for Various Applications II		
	12:10-13:20	Lunch (5F, Tamna B+C)								
	13:20-15:00	**FA3**	**FB3**		**FD3**	**FE3**	**FF3**	**FG3**		
		Microwave Circuits and Systems	Numerical Modelling and Analysis for RF Components and Antennas		SIW and Waveguide-Based Circuits	Compact, Wideband, and Multifunctional Passive Microwave Components	Wireless Power Transfer, RF Devices & Circuit Modeling	[SS] Wireless Power Transmission Regulation, Technology and Industry Trends		
	15:00-15:20	Coffee Break								
	15:20-17:00	**FA4**			**FD4**	**FE4**	**FF4**	**FG4**		
		[SS] Wireless Power Transmission Systems			Electromagnetic Scattering	Milimeter-Wave Components and Packaging Technologies	Emerging Devices and Materials for RF Systems	[SS] Application for Radio Communication		

Organizer KIEES Korean Institute of Electromagnetic Engineering and Science **Co-Organizer** National Radio Research Agency IITP Institute of Information & Communications Technology Planning & Evaluation

Technical Sponsors IEEE MTT-S IEEE AP-S EuMA EiC

Supported by

KOREA TOURISM ORGANIZATION 한국관광공사 · 제주관광공사 JEJU TOURISM ORGANIZATION · Anritsu Advancing beyond · Chang Woo, Inc. · LIG · Hanwha Systems · WAVICE · ROHDE&SCHWARZ · 泰莱微波 Talent Microwave · KCA Korea Communications Agency · TMYTEK · MICROWAVE AT · HzBeat · Qualwave · dbdesign · RXSPACE · KEYSIGHT · RT-Tech 주식회사 알티테크 · QSI Quantum Semiconductor International · 华合半导体 HUA HE SEMICONDUCTOR · KETI Korea Electronics Technology Institute · Shoufei Electronics · MDPI · MMII Laboratory · MPI CORPORATION · withwave

KIEES
The Korean Institute of Electromagnetic Engineering and Science
Address: 101-1101 Lotte Castle President, 109 Mapo-daero, Mapo-gu, Seoul 04146, Republic of Korea
Business Registration Number: 105-82-07643 / Name of Representative: Jae-Sung Rieh

APMC 2025 Secretariat
Genicom, Co., Ltd. 273, Baeul 1-ro, Yuseong-gu, Daejeon 34036, Korea
Tel: +82-42-472-7460 / Fax: +82-42-472-7459 / E-mail: secretariat@apmc2025.org

Session Title:	[WF2] Sub-THz Communication for 6G
Session Date:	December 3 (Wed.), 2025
Session Time:	15:40-17:20
Session Room:	Room F (302)
Session Chair(s):	Doohwan Lee (NTT, Japan) Daekeun Yoon (Kumoh National Institute of Technology, Korea)

[WF2-1] [Invited] 15:40-16:00

Modulation Linearity of Si Mach-Zehnder Modulators

Woo-Young Choi, Min-Hyeok Seong and Yongjin Ji (Yonsei University, Korea (South))

[WF2-2] [Invited] 16:00-16:20

Multishape Radio: Advanced Electromagnetic Wave Manipulation for Enabling 6G Wireless Communications

Doohwan Lee (NTT, Japan); Hirofumi Sasaki and Yasunori Yagi (NTT Corporation, Japan); Kosuke Suzuoki (Nippon Telegraph and Telephone Corporation, Japan); Riichi Kudo (NTT Corporation, Japan)

[WF2-3] 16:20-16:40

A 300-GHz Quartz Transmitarray Using FP Polarizers for Point-to-Point Communications

Jia-Hui Zhao, Feng Xie, Chen-Yu Ding and Zhang-Cheng Hao (Southeast University, China)

[WF2-4] 16:40-17:00

Long-Range Prediction of E-Band OAM Beam Profiles Using Measurement-Based Infinitesimal Dipole Modeling

SeokJu Moon and EunMi Choi (Ulsan National Institute of Science and Technology (UNIST), Korea (South)); Jaehoon Jeong (ETRI, Korea (South)); Young Dam Kim (Chungnam National University, Korea (South))

[WF2-5] 17:00-17:20

A 7.0 pA/√Hz Ultra Low Noise Transimpedance Amplifier with 26.5 GHz Bandwidth for 50G PON

Kunming Yang (Southeast University, China & Institute of Radio Frequency and Optoelectronic Integration, China); Heyu Miao, Fan Yang and Yi Liu (Southeast University, China); Ying mei Chen (SEU, China)

Modulation Linearity of Si Mach-Zehnder Modulators

Woo-Young Choi[#1], Min-Hyeok Seong[#2], Yongjin Ji[#3]

[#]Department of Electrical and Electronic Engineering, Yonsei University, Republic of Korea
{[1]wchoi, [2]alsguree, [3]yjji0314}@yonsei.ac.kr

***Abstract* — Microwave photonics (MWP) is an interdisciplinary field that combines microwave engineering and photonics to generate, process, and distribute high-frequency microwave and millimeter-wave signals using optical components. It enables wide bandwidth, low loss, and immunity to electromagnetic interference, making it ideal for applications in communication, radar, and sensing systems. The Si Mach-Zehnder modulator (MZM) is a critical optical device for many MWP applications. In this paper, a new modeling technique for the Si MZM is presented. The technique includes characteristics of both traveling-wave (TW) electrodes and Si PN junction phase shifters. The modeling accuracy is confirmed by the third-order intermodulation distortion (IMD3) measurement of a Si MZM fabricated by a foundry service.**

***Keywords* — microwave photonics, Si Mach-Zehnder modulators, modulation linearity, third-order intermodulation distortion**

I. Introduction

The recent demands of emerging communication systems, such as 6G and Internet of Things (IoT), are driving the research and development of communication networks that utilize broader and higher frequency bands [1]. Although electronic methods have been widely employed to meet these requirements, they exhibit limitations due to bandwidth constraints as the operating frequency increases. Moreover, electronic systems face additional challenges in high-frequency applications, including limited tunability and inherent signal losses. Microwave photonics (MWP) offers a promising solution to overcome these issues. Using optical devices, it is possible to achieve low transmission loss and wide bandwidth, thereby addressing the limitations.

Si photonics is an emerging platform that enables the integration of photonic components on a Si substrate using standard CMOS-compatible fabrication processes for MWP applications [2]. This technology leverages the transparency of Si in the near-infrared wavelengths (particularly around 1310 nm and 1550 nm), which are widely used in optical communication systems. The primary advantage of Si photonics includes high integration density, compatibility with electronic-photonic co-design, and potential for monolithic integration of photonics and electronics. By utilizing existing semiconductor infrastructure, Si photonics offers a scalable and cost-effective solution for high-bandwidth, low-power optical interconnects in data centers, high-performance computing systems, and emerging quantum and neuromorphic technologies [3].

The high-performance optical modulator is an essential component for many optical signal transmission and processing systems. In MWP applications in which photonics is used for performance enhancement of microwave systems such as photonic microwave filters [4] and photonic analog-to-digital converters [5], optical modulators play a critical role in converting high-frequency electrical signals into the optical domain. For these MWP applications, modulation linearity is the key device characteristic that directly affects overall system performance. Third-order intermodulation distortion (IMD3) and spurious-free dynamic range (SFDR) are widely used as key figures of merit for assessing linearity.

Among various optical modulators realized on the Si photonics platform, Si Mach–Zehnder modulators (MZMs) have emerged as a promising candidate. There have been many reports for many high-performance Si MZMs for digital modulation [6], [7]. However, realization of high-performance Si MZMs for analog applications needs further research and development and, for this, accurate modeling and characterization of the Si MZM are essential.

Previous studies have addressed Si MZM linearity using both simulations [8] and experimental measurements [9]. In particular, [8] used the Taylor series expansion method to model the transfer function and characterize the linearity of Si MZMs, but its complexity limits practical usability.

In this paper, we present a comprehensive modeling technique for evaluating the linearity of Si MZMs. Our approach incorporates the electrical and optical characteristics of both the phase shifters and traveling-wave (TW) electrodes. Model parameters are extracted through simulation and experimental measurement, enabling accurate prediction of fundamental and IMD3 signal power for a given device. The accuracy of this approach is validated using a fabricated Si MZM. Details of these results are given in [10].

II. Si MZM Linearity Model

A Si MZM integrates TW electrodes for microwave signal delivery and PN-junction-based Si phase shifters for optical signal propagation and modulation. The linearity of the Si MZM is affected by several critical factors, including the nonlinear dependence of effective index and junction capacitance of the Si phase shifter on the applied bias voltage, as well as the transmission-line characteristics of the TW electrodes. Fig. 1 illustrates these factors that are carefully analyzed in our investigation.

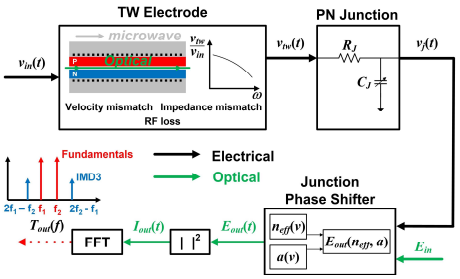

Fig. 1. Block diagram of the linearity model of Si MZMs in this research [10].

When a two-tone sinusoidal input voltage signal $v_{in}(t)$, which has angular frequency near ω, propagates through the TW electrodes, $v_{in}(t)$ experiences modifications due to impedance mismatches between the source, load, and electrode characteristic impedances; velocity mismatch between the optical and microwave signals; and microwave losses in the TW electrodes. [11] provides a model describing the average voltage $v_{avg}(\omega)$, which the optical signal experiences due to these three factors, with the following equation.

$$v_{avg}(\omega)=v_g\cdot\frac{\exp(j\beta_o(\omega)L_{tw})\cdot(1+\Gamma_g(\omega))\cdot(V_+(\omega)+\Gamma_l(\omega)\cdot V_-(\omega))}{(\exp(j\beta_e(\omega)L_{tw})+\Gamma_l(\omega)\cdot\Gamma_g(\omega)\cdot\exp(-j\beta_e(\omega)L_{tw}))}. \quad (1)$$

Here, v_g is the amplitude of $v_{in}(t)$, and L_{tw} is the length of the TW electrode. Γ_g and Γ_l are the reflection coefficients at the termination load and the microwave signal source each, which are given as

$$\Gamma_l(\omega)=\frac{Z_L-Z_o(\omega)}{Z_L+Z_o(\omega)},\ \Gamma_g(\omega)=\frac{Z_o(\omega)-Z_g}{Z_o(\omega)+Z_g}. \quad (2)$$

In the above equations, Z_o is the characteristic impedance of the TW electrode, and Z_L is the load resistance. Z_g is the microwave source impedance, which is 50 Ω. V_+ and V_- are represented by [11]

$$V_\pm(\omega)=\exp\left(\pm j\frac{\beta_e(\omega)\mathrm{m}\beta_o(\omega)}{2}L_{tw}\right)\cdot\frac{\sin\left(\frac{\beta_e(\omega)\mathrm{m}\beta_o(\omega)}{2}L_{tw}\right)}{\frac{\beta_e(\omega)\mathrm{m}\beta_o(\omega)}{2}L_{tw}}, \quad (3)$$

where β_o and β_e are the propagation constants of the optical and the microwave signal, respectively. These are given as

$$\beta_o(\omega)=\frac{\omega}{c}n_o,\ \beta_e(\omega)=-j(\alpha(\omega)+j\frac{\omega}{c}n_{mw}(\omega)), \quad (4)$$

where α is the microwave attenuation coefficient, and n_{mw} is the microwave index of the TW electrode. n_o is the group index of the optical signal passing through the PN-doped Si waveguide.

When $v_{in}(t)$ is introduced to the TW electrode, the effect of the TW electrode can be modeled with $v_{tw}(t)$ given as

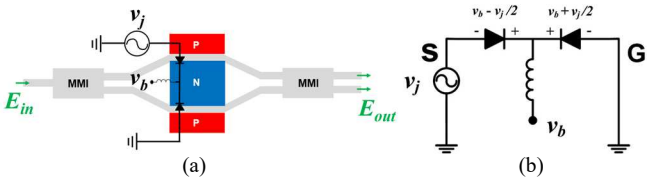

Fig. 2. (a) Block diagram of the structure of the Si SPPMZM and (b) equivalent DC circuit schematic of modulation section of the Si SPPMZM [10].

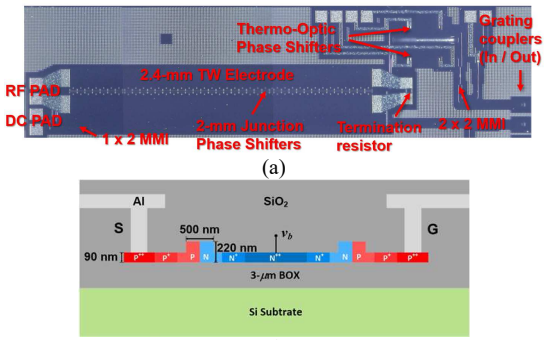

Fig. 3. (a) Microphotograph of the fabricated Si SPPMZM and description of each part and (b) cross-section diagram of the junction phase shifters of the Si SPPMZM [10].

$$v_{tw}(t)=v_{in}(t)\cdot\left|\frac{v_{avg}(\omega)}{v_{avg}(0)}\right|. \quad (5)$$

(5) represents that $v_{in}(t)$ is modified with the scaling factor influenced by the TW effect. When ω of $v_{in}(t)$ is small, the TW effect is small. However, $v_{in}(t)$ can be significantly scaled, if ω is large.

As illustrated in Fig. 1, the signal $v_{tw}(t)$ is additionally affected by the junction resistance R_J and the voltage-dependent junction capacitance C_J of the Si waveguide. $v_j(t)$, which is applied to the PN-doped Si waveguide, induces variations in the effective refractive index $n_{eff}(v)$ and the optical absorption coefficient $a(v)$ of the waveguide, because of the plasma dispersion effect. Assuming a differential drive with zero bias voltage applied to the Si MZM, the output electric field $E_{out}(t)$ of the Si MZM can then be described as follows:

$$E_{out}=\frac{1}{2}\cdot E_{in}\cdot\left[j\cdot\exp(-a(-v_j/2)L_m)\cdot\exp\left(-j\frac{2\pi n_{eff}(-v_j/2)}{\lambda}L_m\right)\cdot\exp(-j\phi)+\exp(-a(v_j/2)L_m)\cdot\exp\left(-j\frac{2\pi n_{eff}(v_j/2)}{\lambda}L_m\right)\right]. \quad (6)$$

L_m is the length of the PN junction phase shifter. ϕ is the initial optical phase difference between two arms of the Si MZM. The intensity of the modulated optical signal, $I_{out}(t)$, can be obtained from $E_{out}(t)$, and this can be converted into the power spectral density, $T_{out}(f)$, from which the fundamental and IMD3 signals of the Si MZM can be determined.

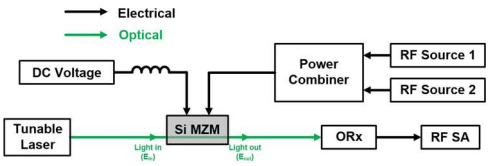

Fig. 4. Setup used in measurement of the Si SPPMZM linearity for the verification of the linearity simulation model. ORx: optical receiver, RF SA: RF spectrum analyzer [10].

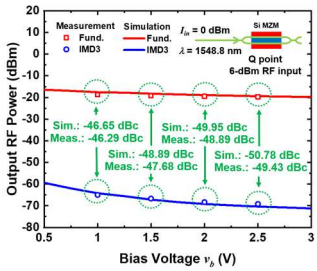

Fig. 5. Simulated and measured values of fundamental and IMD3 signals along v_b. The input optical power applied to the Si SPPMZM is 0 dBm. The used wavelength is 1548.8 nm. Input microwave power is 6 dBm. The bias point is quadrature point [10].

III. A Sample Si MZM

To validate the accuracy of the linearity model described above, a Si single-ended push-pull MZM (SPPMZM), whose structural design is depicted in Fig. 2(a), was fabricated in a Si photonics foundry. A reverse bias voltage v_b is applied to the shared N-type region of the two phase shifters via an inductor. This external inductor, part of a commercial Bias-T, blocks the microwave signal from leaking into the bias line, thereby enabling proper push-pull operation of the Si SPPMZM. When a microwave signal v_j is applied to one of the P-type regions, labeled S, it encounters two series-connected capacitors. As a result, the voltages $v_b - v_j/2$ and $v_b + v_j/2$ are applied across the two respective PN junctions. This configuration allows the Si SPPMZM to modulate the optical signal in a differential manner using a single microwave input, as illustrated in Fig. 2(b).

Fig. 3(a) illustrate the chip photograph of the Si SPPMZM. The Si SPPMZM has 2-mm PNP-doped junction phase shifters. A termination resistor is placed at the end part of the TW electrode. Both arms of the Si SPPMZM have thermo-optic heaters, with which the MZM bias point is thermally tuned. Grating couplers are used for optical I/O. Fig. 3(b) displays the cross-section of the PN junction phase shifters in the Si SPPMZM.

IV. Experimental Verification

Fig. 4 illustrates the setup used to measure the IMD3 of the Si SPPMZM for validating the proposed linearity simulation model. Two RF signal generators (Anritsu 68177C and Agilent 83752B) and a power combiner (Mini-Circuits ZX10-2-183-S+) are used to generate and deliver a two-tone microwave signal to the Si MZM. The optical signal output from the modulator is converted to an electrical signal using an optical receiver (Optilab PR-23-M), and the resulting microwave signal power spectrum is analyzed by a spectrum analyzer (Agilent 8593E). Both simulation and experimental measurements use two-tone sinusoidal signals at 9.9 GHz and 10.1 GHz. A wavelength of 1548.8 nm is chosen for the measurement to minimize coupling loss through the grating couplers. The input optical power to the Si SPPMZM is set at 0 dBm, and the device is mounted on a temperature-controlled stage maintained at 25 °C.

Fig. 5 shows the simulated and measured results of the fundamental and IMD3 components as a function of v_b, when the Si SPPMZM is biased at the quadrature point, where half of the input optical power is transmitted. The simulated and experimental results are in good agreement, with a maximum discrepancy of no more than 1.5 dB. This low difference between the measured and simulated results indicates the high accuracy of our modeling technique.

V. Conclusion

We presented a modeling technique with which the linearity characteristics of Si MZMs can be precisely analyzed. Our model includes the effects of the optical characteristics of the PN junction phase shifters as well as the transmission characteristics of the TW electrodes. Using this modeling technique, fundamental and IMD3 signal power of Si MZMs can be determined, and the accuracy of the model is confirmed with the measurement results.

References

[1] J. Capmany and D. Novak, “Microwave photonics combines two worlds,” *Nature Photonics*, vol. 1, no. 6, p. 319, 2007, doi: https://doi.org/2010.1038/nphoton.2007.89.

[2] L. R. Chen, "Silicon photonics for microwave photonics applications," *J. Lightw. Technol.*, vol. 35, no. 4, pp. 824-835, 2017, doi: https://doi.org/10.1109/JLT.2016.261386.

[3] Y. Shen *et al*., "Silicon photonics for extreme scale systems," *J. Lightw. Technol.*, vol.37, no.2, pp. 245-259, 2019, doi: https://doi.org/10.1109/JLT.2019.2897365.

[4] M. Gutierrez *et al*., “A photonic microwave filter based on an asymmetric silicon Mach-Zehnder modulator,” *IEEE Photon. J*., vol. 5, no. 4, Aug. 2013, doi: https://doi.org/10.1109/JPHOT.2013.2269677.

[5] A. Khilo *et al*., “Photonic ADC: Overcoming the bottleneck of electronic jitter,” *Opt. Exp.*, vol. 20, no. 4, pp. 4454 –4469, Feb. 2012, doi: https://doi.org/10.1364/OE.20.004454.

[6] C. Han *et al*., “Slow-light silicon modulator with 110-GHz bandwidth,” *Science Advances*, vol. 9, no. 42, 2023, doi: https://doi.org/10.1126/sciadv.adi5339.

[7] X. Wang *et al*., “High-speed silicon photonic Mach-Zehnder modulator at 2 μm,” Photon. Res., vol. 9, no. 4, pp. 535-540, 2021, doi: https://doi.org/10.1364/PRJ.417107.

[8] Q. Zhang *et al.*, “Linearity comparison of silicon carrier-depletion-based single, dual-parallel, and dual-series Mach–Zehnder modulators,” *J. Lightw. Technol.*, vol. 36, no. 16, pp. 3318–3331, Aug. 2018, doi: https://doi.org/10.1109/JLT.2018.2839603.

[9] Y. Zhou *et al*., "Linearity measurement and pulse amplitude modulation in a silicon single-drive push–pull Mach–Zehnder modulator," *J. Lightw. Technol.*, vol. 34, pp. 3323-3329, 2016, doi: https://doi.org 10.1109/JLT.2016.2567067.

[10] M.-H. Seong *et al*., “Modulation linearity characterization of Si Mach-Zehnder modulators,” *J. Lightw. Technol.*, vol. 42, no. 6, pp. 1901-1909, Mar. 2024, doi: https://doi.org/10.1109/JLT.2023.3327146.

[11] Y. Zhou *et al*., "Modeling and optimization of a single-drive push–pull silicon Mach–Zehnder modulator," *Photon. Res.*, vol. 4, 153-161, Aug. 2016, doi: https://doi.org/10.1364/PRJ.4.000153.